Earth and Planetary Science Letters 611 (2023) 118148

Contents lists available at ScienceDirect

Earth and Planetary Science Letters

journal homepage: www.elsevier.com/locate/epsl

Mantle plume heat flux and surface motion periodicities and their implications for the growth of continental crust

Mingming Li [a,*], Stephen Puetz [b], Kent Condie [c], Peter Olson [d]

[a] School of Earth and Space Exploration, Arizona State University, Tempe, AZ, USA
[b] Progressive Science Institute, Honolulu, HI, USA
[c] Department of Earth & Environmental Science, New Mexico Institute of Mining and Technology, Socorro, NM, USA
[d] Department of Earth and Planetary Sciences, University of New Mexico, Albuquerque, NM, USA

ARTICLE INFO

Article history:
Received 19 October 2022
Received in revised form 23 March 2023
Accepted 28 March 2023
Available online xxxx
Editor: H. Thybo

Keywords:
growth of continental crust
3D global geodynamic models
mantle plumes
heat flux
periodicity
surface velocity

ABSTRACT

About 40% of Earth's surface is covered by continental crust. It has been found that the global detrital zircon age distribution is dominated by multiple periodicities from <100 Myr to ~800 Myr, suggesting that continental crust may have been produced periodically. However, what causes the periodic growth of continental crust remains unclear. Continental crust is produced mainly by arc magmatism at subduction zones and plume-induced magmatism. With 3D global mantle convection models, we investigate the long-term evolution of heat flux of mantle plumes and surface flow velocity, which can be respectively related to plume-induced magmatism and arc magmatism. About 10-30 plumes are present in our models, with significant spatial and temporal variations of heat flux for individual plumes. Both the temporal variations of the total plume heat flux and the root-mean-square (rms) of the surface velocity in our models have periodicities that decrease with the vigor of mantle convection. When extrapolated to conditions with Earth-like vigor of convection, the total plume heat flux and the rms of the surface velocity vary with periodic cycles of ~90-200 Myr and ~300 Myr, respectively. Therefore, the ~90-200 Myr and the ~300 Myr periodic cycles in the growth of continental crust as suggested by the global detrital zircon age distribution may be respectively caused by plume-induced magmatism and arc magmatism.

1. Introduction

~40% Earth's surface area is covered by continental crust, but how the volume of continental crust grows with time remains under debate (e.g., Armstrong and Harmon, 1981; Rudnick, 1995; Albarède, 1998; Condie and Aster, 2010; Arndt and Davaille, 2013; Condie et al., 2017). Recently, U-Pb ages of detrital zircons have been compiled on a global scale, with samples assigned a weight inversely proportional to regional surface areas (Condie et al., 2017; Puetz and Condie, 2019, 2022). Fig. 1 shows the global detrital zircon U-Pb age distribution, or A_{zir}, compiled by (Puetz and Condie, 2019), and the periodogram of A_{zir} at 3000-0 Ma. Results show the A_{zir} peaks at multiple periodicities ranging from less than ~100 Myr to ~ 800 Myr at/above the 95% confidence interval. These periodicities have been systematically tested by Puetz and Condie (2022) via spectral analysis on four independent global detrital zircon databases (Voice et al., 2011; Roberts and Spencer, 2015; Puetz and Condie, 2019; Puetz et al., 2021), and they found that each time-series had a multitude of nearly identical periodicities above the 95% confidence level. Because these detrital zircon periodicities are consistently reproducible at high confidence levels from four independent databases, they are very likely real periodicities. The question is: what causes these periodicities?

Continental crust is produced mainly by arc magmatism at subduction zones and intra-plate magmatism above mantle plumes (e.g., Rudnick, 1995; Albarède, 1998). It is recycled into the deep mantle through processes of subduction erosion, sediment subduction and lower-crustal delamination (e.g., Armstrong and Harmon, 1981). The present-day volume of continental crust thus reflects a balance between crustal production, storage, and recycling. Interestingly, it has been found that U–Pb age distribution of zircons from igneous rocks shows peaks at 2700, 2500, 2100, 1900, 1750, 1100, and 600 Ma and probably at 3450, 3000, 2000, and 300 Ma (Condie and Aster, 2010; Condie et al., 2014). Arndt and Davaille (2013) showed that these peaks can be explained by accelerated

* Corresponding author.
E-mail address: mingming.li@asu.edu (M. Li).

https://doi.org/10.1016/j.epsl.2023.118148
0012-821X/

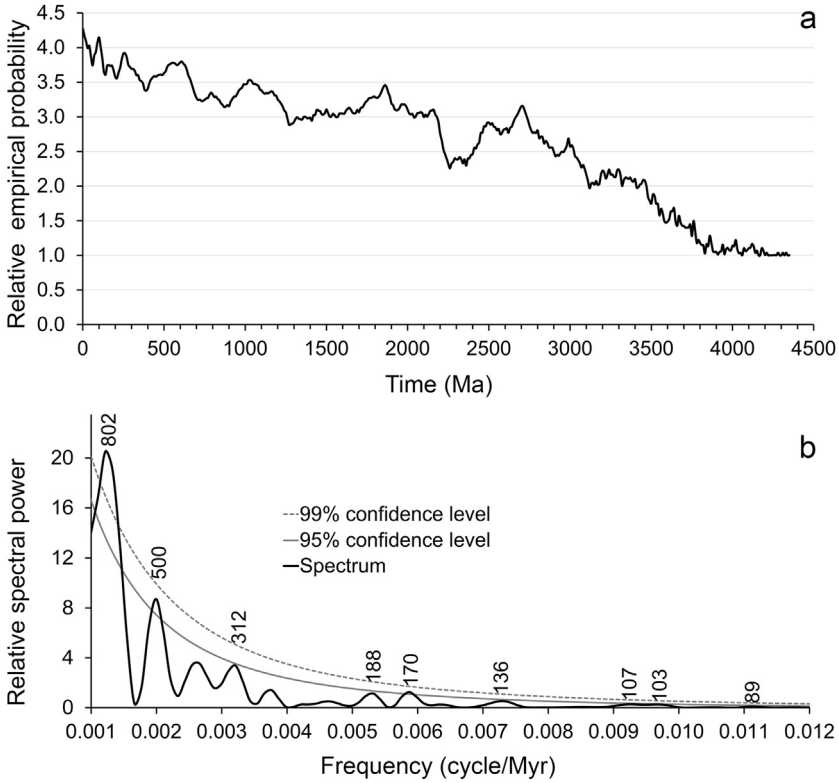

Fig. 1. a, Time evolution of global detrital zircon U-Pb age distribution A_{zir} (Puetz and Condie, 2019). b, The power spectral of the data in panel (a). Numbers above the peaks refer to periodicities whose magnitude are at/above the 95% confidence level. Spectral analysis is performed for the time interval of 3000-0 Ma after linear trend is removed.

crustal production related to episodic convection of the mantle, although the peaks post 1000 Ma coincide with times of supercontinent assembly and may represent periods of enhanced crustal preservation (Hawkesworth et al., 2010; Stern and Scholl, 2010). Therefore, the periodicities of U-Pb detrital zircon age distribution may mostly represent periodicities in the production of continental crust. The question is: what leads to periodic production of continental crust? Since continental crust is mainly produced by arc-magmatism at subduction zones and plume-induced magmatism, it is critical to understand the temporal variations of the formation of mantle plumes and the subduction rate in Earth's history. Are these variations periodical in nature? If so, are the periodicities similar to that of the global zircon age distribution?

Mantle plumes form from a thermal boundary layer (TBL), e.g., the core-mantle boundary (CMB) and rise towards the surface, and often reach the uppermost mantle. Linear stability theory (Howard, 1966; Olson, 1993) predicts that, as a TBL thickens due to thermal diffusion, the local Rayleigh number increases and when it reaches a critical value, the TBL becomes unstable and forms thermal instabilities - which eventually develop into upwelling thermal plumes. Plume formation times and the periodicity of plume heat flux are significantly controlled by mantle viscosity. A period of ~100-200 Myr is predicted in the models of Li et al. (2018) after scaling to Earth-like vigor of convection.

In addition, periodicity of heat flux has been predicted for thermochemical plumes that have different composition than the surrounding mantle (Le Bars and Davaille, 2004; e.g., Davaille et al., 2005; Lin and van Keken, 2005). Numerical experiments have shown that entrainment of intrinsically dense materials by a plume from the lowermost mantle can produce multiple episodes of thermal instabilities (Lin and van Keken, 2005) with the time between neighboring episodes varying with viscosity and the intrinsic density of the materials. Laboratory experiments have shown thermochemical plumes with alternating phases of sinking and rising (e.g., Le Bars and Davaille, 2004; Davaille et al., 2005), and when extrapolated to mantle conditions, the periodicities of this behavior are ~100-200 Myr (Le Bars and Davaille, 2004; Davaille et al., 2005).

Although the heat flux of a single plume may vary periodically, the periodic variation can be interrupted or destroyed by changes of mantle dynamics that cause perturbations to the TBL (Li and Zhong, 2017; Li et al., 2018; Heyn et al., 2020). In fact, a single plume does not last forever: it can move, disappear, or merge with other plumes (Li and Zhong, 2019; Arnould et al., 2020). In addition, dozens of mantle plumes have been proposed to exist in Earth's mantle, which may have a variety of thermal structures, dynamics, and perhaps lifespans (Sleep, 1990; Davies, 1993; Courtillot et al., 2003). Therefore, it remains unclear whether the total heat flux of mantle plumes, and thus the plume-induced magmatism, can vary periodically.

Besides mantle plumes, continental crust is also produced by arc volcanism above subduction zones (Rudnick, 1995; Hawkesworth et al., 2010). It has been proposed that pulses of continental crust growth may result from periods of accelerated plate motion during most of Earth's history (O'Neill et al., 2007; Arndt and Davaille, 2013). However, the effect of periodicities of the long-term variation of plate motion has not yet been fully investigated in 3D global mantle convection models. It also remains unclear to what extent these periodicities agree with those of the global detrital zircon age data.

Here, we perform 3D global mantle convection models to study the long-term variations of plume heat flux and surface motion. In our models, thermal plumes form naturally from thermal instabilities at the basal TBL above the CMB and then rise towards the surface. All models are run for 4.5 Gyr. We perform spectral analyses on the secular variations of the total plume heat flux and the rms of the surface velocity in our models. We examine periodicities that are lower than 1,000 Myr and compare them with those

of the global detrital zircon age data which range from <100 Myr to ~800 Myr (Fig. 1b).

2. Methods

We solve the following conservation equations of mass, momentum, and energy under the extended-Boussinesq approximation:

$$\nabla \cdot \vec{u} = 0, \tag{1}$$

$$-\nabla P + \nabla \cdot (\eta \dot{\epsilon}) + (\mathrm{Ra}\alpha \mathrm{T} + \mathrm{Ra_p}\Gamma_\mathrm{p})\hat{r} = 0, \tag{2}$$

$$\left[1 + \gamma^2 \frac{Ra_p}{Ra}\frac{d\Gamma}{d\pi} D_i (T + T_s)\right]\left(\frac{\partial T}{\partial t} + \vec{u} \cdot \nabla T\right) + \left(\alpha + \gamma \frac{Ra_p}{Ra}\frac{d\Gamma}{d\pi}\right)(T + T_s) D_i u_r = \nabla \cdot (\kappa \nabla T) + \frac{D_i}{Ra}\sigma_{ij}\frac{\partial u_i}{\partial x_j} + H, \tag{3}$$

where $\vec{u}$, P, η, $\dot{\epsilon}$, Ra, α, T, T_s, D_i, κ, σ_{ij}, and H are, respectively, the velocity, dynamic pressure, viscosity, strain rate, Rayleigh number, thermal expansivity, temperature, surface temperature, dissipation number, thermal diffusivity, deviatoric stress, and internal heating rate; $\hat{r}$ is a unit vector in radial direction, u_r is the radial velocity, t is time; γ is the Clapeyron slope for the phase transition at 660 km depth and Ra_p, Γ and π are the corresponding Rayleigh number, phase function, and excess pressure for this phase transition. Eq. (1)-(3) are non-dimensional, and they are derived using the following characteristic scales linking dimensional (primed) and non-dimensional variables (not primed):

$$x_i' = x_i R, \tag{4}$$

$$u_i' = \frac{u_i \kappa_0}{R}, \tag{5}$$

$$T' = \Delta T\,(T + T_s), \tag{6}$$

$$t' = t\frac{R^2}{\kappa_0}, \tag{7}$$

$$\eta' = \eta\eta_0, \tag{8}$$

$$P' = P\frac{\eta_0 \kappa_0}{R^2}, \tag{9}$$

$$\gamma' = \gamma\frac{\rho g R}{\Delta T}, \tag{10}$$

$$H' = H\frac{C_p \kappa_0 \Delta T}{R^2}, \tag{11}$$

where x_i is length, R is Earth's radius, κ_0 is surface thermal expansivity, ΔT is temperature change across the mantle, η_0 is reference viscosity, ρ is reference density, g is gravitational acceleration, and C_p is heat capacity. The Eq (1)-(3) are solved using the CitcomS code (Zhong et al., 2008). The model domain ranges from the CMB to the top surface and is divided into 12 equal-volume caps with each cap containing 64×64×64 elements. The values of dimensional physical parameters used in this study are summarized in Supplementary Information Table S1.

The Rayleigh numbers Ra and Ra_p are defined as:

$$Ra = \frac{\rho g \alpha_0 \Delta T R^3}{\kappa_0 \eta_0}, \tag{12}$$

$$Ra_p = \frac{\Delta\rho_{660}}{\rho\alpha_0 \Delta T} Ra, \tag{13}$$

where α_0 is the surface thermal expansivity, and $\Delta\rho_{660}$ is the density increase due to the 660 km depth phase transition. There is a 3× decrease of thermal expansivity and an 2.18× increase of thermal diffusivity from the surface to the CMB (Supplementary Information Table S1), which are consistent with mineral physics studies (Duffy and Ahrens, 1993; Hofmeister, 1999).

The phase function for the 660 km phase transition is defined as:

$$\Gamma(\pi) = 0.5 + 0.5\tanh\left(\frac{\pi}{\delta}\right), \tag{14}$$

where δ is the width of the phase transition and the excess pressure π is defined as:

$$\pi = d - d_{660} - \gamma(T - T_{660}), \tag{15}$$

where, d is the depth, d_{660} and T_{660} are the reference depth and temperature for the phase transition at 660 km depth, and again, γ is the Clapeyron slope.

The mantle viscosity is both temperature and depth dependent, which is defined as:

$$\eta = \eta_r \exp\left[E\,(0.5 - T) + V(1 - r_d)\right], \tag{16}$$

where E is the coefficient of activation energy for temperature-dependent viscosity and V=3.0 is the coefficient of activation volume which leads to ~4× increases of viscosity due to the increase of depth or pressure from the surface to the CMB, r_d is radius, and η_r is a prefactor which is 10.0 at 0 – 150 km depth, 1.0 at 150 – 660 km depth, and 30.0 from 660 km depth to the CMB. This viscosity law leads to a relatively strong lithosphere and an 30× increase in viscosity from the upper mantle to lower mantle across the 660 km discontinuity. In addition, plastic deformation is included in our models by introducing a yield stress above which the viscosity is modified by:

$$\eta_{new} = 1/\left[\frac{1.0}{\eta} + \frac{1.0}{\eta_{yield}}\right], \tag{17}$$

$$\eta_{yield} = \frac{\tau_{yield}}{D}, \tag{18}$$

where η_{yield} is the viscosity related to yield stress τ_{yield} under the second invariant of strain rate D. We assume a constant value of τ_{yield}=10^6 (non-dimensional) or 102 MPa in the uppermost 150 km of our models. This simplified approach is used only to break a stagnant lid to have mobile-lid convection, but not meant to capture all complexities of the lithospheric deformation which remains challenging to model.

Both the surface and the CMB are free-slip and have constant temperatures of T=0 (or 0 °C) and T=1 (or 3300 °C), respectively. All models are run for 4.5 Gyr. The temperature and velocity fields are saved every 1 to 6 Myr for post-processing. Geological records have suggested an average mantle potential temperature T_{pot} (the extrapolated temperature at the surface following adiabatic gradient) of ~1400 °C at present-day and ~1600 °C at ~3.0 Ga (Abbott et al., 1994; Herzberg et al., 2010; Dalton et al., 2014). To obtain an appropriate initial temperature condition at 4.5 Ga, we first test a model in which we vary the internal heating rate to allow the mantle to reach a T_{pot} of 1650 °C or 1710 °C. The temperature field of this model is then used as initial temperature condition for new models. The radiogenic heat production rate is a function of time, defined as:

$$H(t) = H(0)\sum_{n=1}^{4} h_n \exp(\lambda_n t), \tag{19}$$

where $H(0)$ is the radioactive heat production at present-day, λ_n and h_n are constants related to the half-life and concentration of

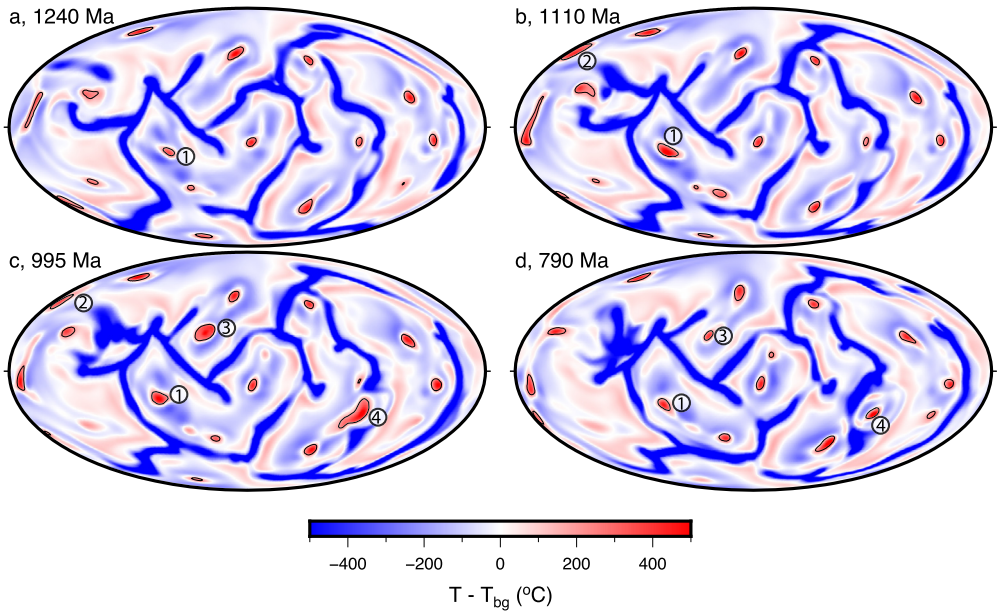

Fig. 2. Snapshots of residual temperature at 700 km depth after the background temperature T_{bg} is removed at 1240 Ma (a), 1110 Ma (b), 995 Ma (c), and 790 Ma (d) for case 1. Red spots are plume regions with δT_{plume}>200 °C. Four plumes with numbers nearby are selected for description in the main text.

heat producing elements which are adopted from Korenaga (2006) and are listed in Supplementary Information Table S2, and t is the time before present-day. The $H(0)$ is varied in each model such that T_{pot} generally decreases with time from 1650 °C or 1710 °C at 4.5 Ga to ∼1400 °C at present-day (Supplementary Information Figure S1a).

Like previous work (Zhong, 2006; Leng and Zhong, 2008; Li et al., 2018; Li and Zhong, 2019), thermal plumes are defined at each depth in regions where the radial velocity is positive (or upward) and the temperature satisfies:

$$T > T_{bg} + f, \tag{20}$$

where f is an excess temperature above the background temperature T_{bg}, and the value of $f + T_{bg}$ determines the threshold temperature for plumes. As with previous studies, T_{bg} at each depth is measured by the laterally averaged temperature excluding relatively cold (e.g., downwelling) regions where $T \leq T_{ave}$ with T_{ave} being the laterally averaged temperature. If two or more plumes are within 3 degrees from one another, they are treated as a single plume. Similar to (Zhong, 2006) and (Leng and Zhong, 2008), the heat flux of a single plume at each depth is measured by:

$$q = \int_S \rho C_p u_r (T - T_{bg}) dS, \tag{21}$$

where $T - T_{bg}$ is the plume access temperature (hereinafter denoted as δT_{plume}), S is the area of the plume at this depth, and u_r is the plume radial velocity. Spectral analyses are performed with the REDFIT software (Schulz and Mudelsee, 2002) in which we use Welch's method to remove sideband frequencies.

3. Results

We first present the results for the reference case, case 1, which uses a Rayleigh number of Ra=2×10^8, an initial average mantle potential temperature of T_{pot} =1650 °C, a coefficient of activation energy of E=9.21 which leads to a maximum viscosity change of $10^{4\times}$ as temperature changes from 0 to 1. Note that in this study, Ra is defined using a length scale equal to Earth's radius (Eq. (12)); therefore, it is about 10 times larger than if defined using the mantle thickness as the length scale.

Fig. 2 shows a sequence of snapshots for the residual temperature at 700 km depth after the background temperature is removed. Fig. 3a shows the total plume heat flux or Q_p at this depth as a function of time for case 1. Plumes are defined as regions (red spots with black contours) that satisfy Eq. (20) with f=0.06, e.g., with a threshold of plume excess temperature of δT_{plume}=200 °C. Four thermal plumes are selected in Fig. 2 to illustrate how changes in plume area and temperature affect Q_p. From 1240 Ma (Fig. 2a) to 1110 Ma (Fig. 2b), the area and temperature of plume #1 are both increased, a new plume #2 arrives at this depth, and the Q_p increases from 1.3 TW to 1.9 TW (Fig. 3a). From 1110 Ma (Fig. 2b) to 995 Ma (Fig. 2c), two new plumes #3 and #4 arrive at this depth, and the Q_p further increases to 2.4 TW (Fig. 3a). From 995 Ma (Fig. 2c) to 790 Ma (Fig. 2d), plume #2 disappears, plumes #1, #3 and #4 become smaller, and Q_p is reduced to 1.8 TW (Fig. 3a).

Similar processes as shown in Fig. 2 occur throughout the model run from 4500 Ma to 0 Ma (Supplementary Information Movie S1), with new plumes continually forming and old plumes continually disappearing. About 10-20 plumes are observed at almost every timestep (Supplementary Information Figure S1b), which show a variety of sizes and temperatures, and thus heat flux. The arrival of new plumes and the increase of area and temperature for some pre-existing plumes often correspond to increases of Q_p, whereas decreases in the area and temperature of plumes correspond to reductions of Q_p.

Although the heat flux of a single thermal plume may vary periodically, the time evolution of the total plume heat flux Q_p is more complex. As shown in Fig. 3a (black), the secular variation of Q_p contains a long-term linear increase from ∼0.5 TW at 4500 Ma to ∼3 TW at 0 Ma and other variations occurring over shorter periods. Spectral analysis shows that the variation of Q_p during 3000-0 Ma is dominated by periodicities of 310, 260, 198, and 127 Myr with magnitudes exceeding the 95% confidence interval, with the periodicities of 260, 198, and 127 Myr above the 99% confidence interval (Fig. 3b).

Compared to Q_p, the variation of the root-mean square (rms) of the surface velocity (u_0^{rms}) is much smoother (Fig. 3a, orange)

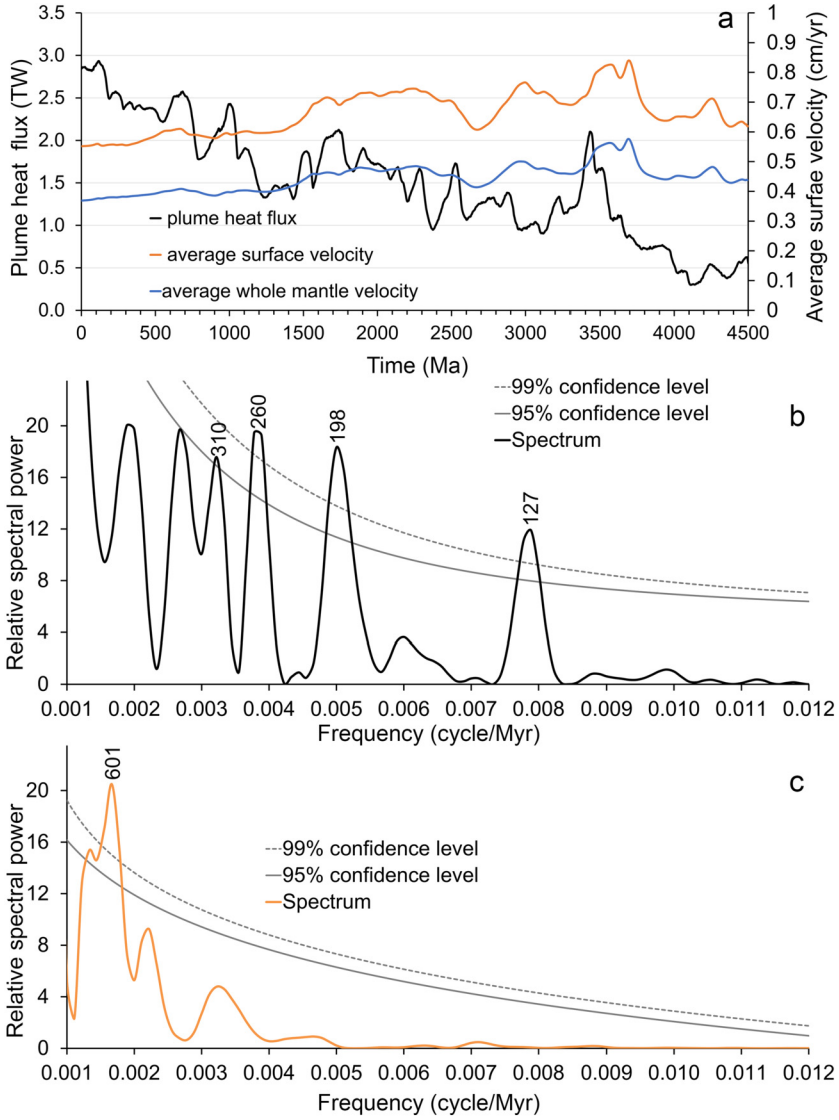

Fig. 3. a, Time evolution of total plume heat flux Q_p at 700 km depth (black), root-mean square of surface velocity u_0^{rms} (orange) and the whole mantle velocity u_{wm}^{rms} (blue) for case 1. Note that the present-day is marked as 0 Ma on the horizontal axis. b, Power spectrum of Q_p. c, Power spectrum of u_0^{rms}. In panels b and c, numbers above the peaks refer to periodicities whose magnitudes are above the 95% confidence level. Spectral analyses are performed at 3000-0 Ma after the linear trends are removed.

and has a periodicity of 601 Myr above the 99% confidence interval (Fig. 3c). The variation of u_0^{rms} follows closely with that of the whole mantle flow velocity u_{wm}^{rms} (Fig. 3a), with a correlation coefficient of r=0.97, suggesting that surface velocity is closely coupled with the deep mantle convection in our models.

The Q_p presented above is calculated at 700 km depth using f=0.06 (e.g., a threshold of plume excess temperature of 200 °C). We find that an increase (decrease) of f leads to a reduction (increase) of plume area and thus a reduction (increase) of Q_p, but the trend and pattern of the variations of Q_p are not affected (Fig. 4a). The Q_p also increases with depth, although the trends and patterns of Q_p variations are not greatly affected, apart from a time shift with radius due to plume rise (Fig. 4b). Figs. 4c-d show the average plume excess temperature and the total plume area as a function of depth at 0 Ma. As shown in Fig. 4c, the plume excess temperature increases with depth. Because plumes at different depths are defined according to Eq. (20) using the same f, the plume radius also increases with depth (Fig. 4d). Therefore, the increase of plume heat flux with depth as shown in Fig. 4b is likely caused by the increase of both plume excess temperature and plume radius. The significant increase of plume heat flux with depth has also been found in Zhong (2006) and Leng and Zhong (2008). However, except for a slight lag in time, we do not observe a reduction of Q_p from 700 km to 300 km. This may be because the diameters of plumes are reduced in the upper mantle due to a reduction of mantle viscosity, and as a result, plume dynamics in the upper mantle is not well resolved due to limits of model resolution. Hereafter, we focus on Q_p in the lower mantle at 700 km where plumes are better resolved.

The temporal variation of Q_p in our models contains a long-term linear increase component (Fig. 3–4), in addition to relatively shorter time-scale variations. Like previous studies (Zhong, 2006; Leng and Zhong, 2008), the plume heat flux in this study is calculated from the production of plume excess temperature δT_{plume}, plume area, and plume radial velocity (Eq. (21)). In our models, the plume temperature is directly controlled by the CMB temperature that is kept constant, but the background mantle cools linearly with time (Fig. 5a). As a result, there is a long-term linear increase of δT_{plume} with time (Fig. 5b). Mantle plumes are defined in regions where the δT_{plume} is larger than a threshold (e.g., the factor f in Eq. (20)), and because of this definition, the linear increase of the δT_{plume} with time leads to a linear increase

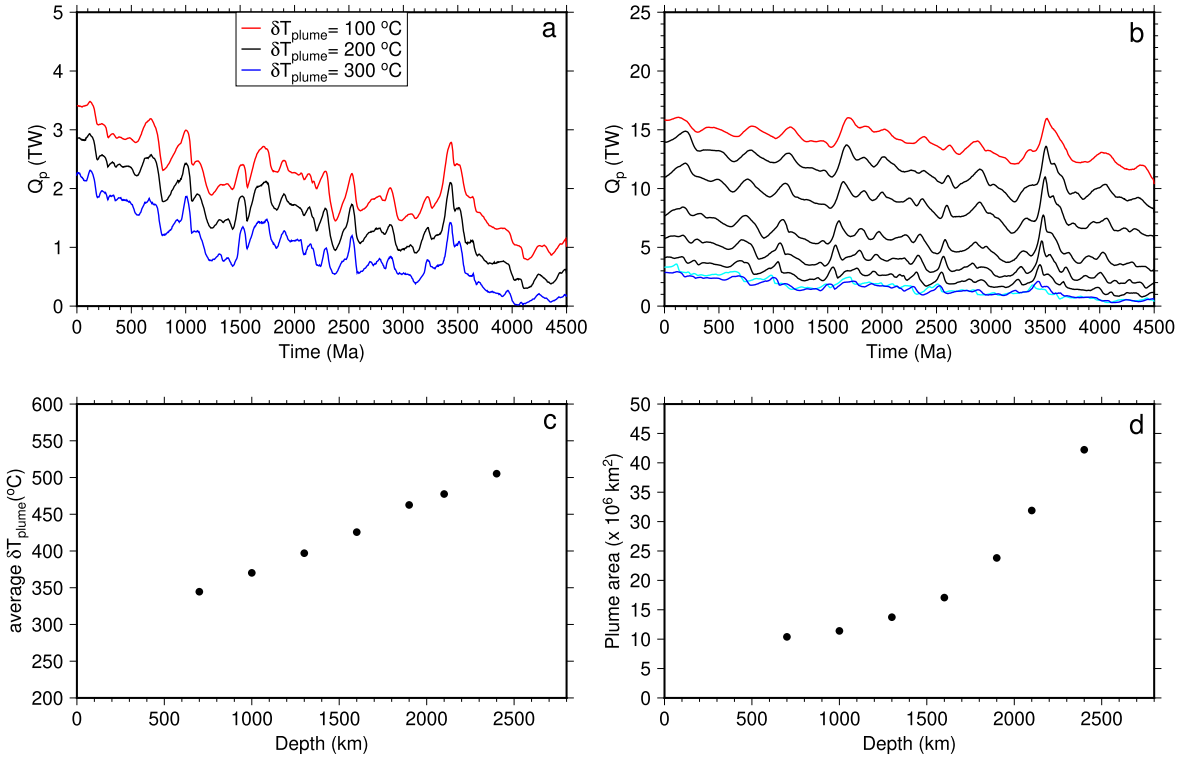

Fig. 4. a, Time evolution of total plume heat flux Q_p at 700 km depth calculated using plume excess temperature of 100 °C with f=0.03 (red), 200 °C with f=0.06 (black), and 300 °C with f=0.09 (blue). b, Time variations of Q_p quantified with f=0.06 at depths of 300 (cyan), 700 (blue), and 2400 km (red). The black curves from bottom to top respectively show Q_p at depths of 1000, 1300, 1600, 1900, to 2100 km. c-d, The average plume excess temperature δT_{plume} (c) and the total plume area at 700, 1000, 1300, 1600, 1900, 2100, and 2400 km depths (d) at 0 Ma.

of plume radius and plume area (Fig. 5c). Furthermore, our models also show a long-term linear increase of plume radial velocity with time (Fig. 5d). The linear increases of δT_{plume} (Fig. 5b), plume area (Fig. 5c), and plume radial velocity (Fig. 5d) together result in a linear increase of the Q_p.

It needs to be pointed out that the Earth's CMB temperature may decrease with time, and if we reduce the CMB temperature with time in our models, we may reduce the linear increase of Q_p. It has also been suggested that T_{pot} for the Earth's mantle may have started with low and reached a maximum in the mid-Archean (~3.0 Ga) and then decrease linearly with time to present-day (Korenaga, 2006; Herzberg et al., 2010). In such case, our results suggest Q_p may first decrease to minimum at mid-Archean before increase with time to present-day. However, the temporal variation of the CMB temperature and the early thermal evolution of the Earth remain not well constrained. Nevertheless, the linear trends in Q_p are removed before we perform spectral analyses. Adding variable CMB temperature will also change the heat source which will, in turn, gradually change the background mantle temperature. The effects of different background mantle on our results are examined later in case 5. Therefore, to avoid including more model uncertainties that do not change our conclusions, we keep the CMB temperature constant in our models and do not explore the possibility of an increase of mantle temperature in the early Earth before ~3.0 Ga.

We also find that, after the linear treads are removed, the shorter timescale variations of the Q_p still correlate well with δT_{plume}, plume area, and plume radial velocity, with correlation coefficients of 0.78, 0.73 and 0.71, respectively (Fig. 5b-d). This result is not surprising because plume heat flux is related to plume area, excess temperature, and radial velocity based on Eq. (21).

In what follows, we explore how plume dynamics and Q_p at 700 km depth can be affected by changes of model parameters - including Rayleigh number, degree of temperature-dependence of viscosity, and initial mantle temperature. For better comparison, the internal heat rate is modified accordingly to ensure all models to have similar mantle potential temperatures that decrease with time from ~1620-1720 °C at 4500 Ma to ~1380-1440 °C at present-day (Supplementary Information Figure S1a, Supplementary Information Table S3).

Case 2 uses the same parameters as case 1 except that the Rayleigh number is reduced to Ra=1×10^8, which is 0.5× that of case 1 (Supplementary Information Table S3). One direct consequence is that mantle convection becomes more stable, as demonstrated by the much smoother changing of u_0^{rms} with time compared to case 1 (Fig. 6a, orange). Only ~2-8 plumes are identified in this case (Supplementary Information Figure S1b). The present-day Q_p for case 2 is ~0.4 TW, which is ~7 times lower than case 1 (Fig. 6a). The secular variation of Q_p for case 2 shows periodicities of 826 Myr and 568 Myr above the 99% confidence level (Fig. 6b), and the variation of u_0^{rms} has a periodicity of 646 Myr above the 99% confidence level (Fig. 6c).

Case 3 uses a Rayleigh number 2× that of case 1 (Supplementary Information Table S3). About 20-30 plumes are found in this case, more than that in case 1 (Supplementary Information Figure S1b). The Q_p in case 3 is higher and varies more strongly and frequently than that in case 1 (Fig. 7a). The variation of Q_p is dominated by periodicities of 227, 134, 121, 89 Myr that are above the 95% confidence level, among which the periodicities of 121 and 89 Myr are above the 99% confidence level (Fig. 7b), and u_0^{rms} has a periodicity of 362 Myr that is above the 99% confidence level (Fig. 7c).

In case 4, the activation coefficient for the temperature-dependence of viscosity is increased to E=13.82 in the lower mantle (Supplementary Information Table S3). Therefore, the viscosity of the basal hot TBL is reduced. The Q_p is higher and varies more

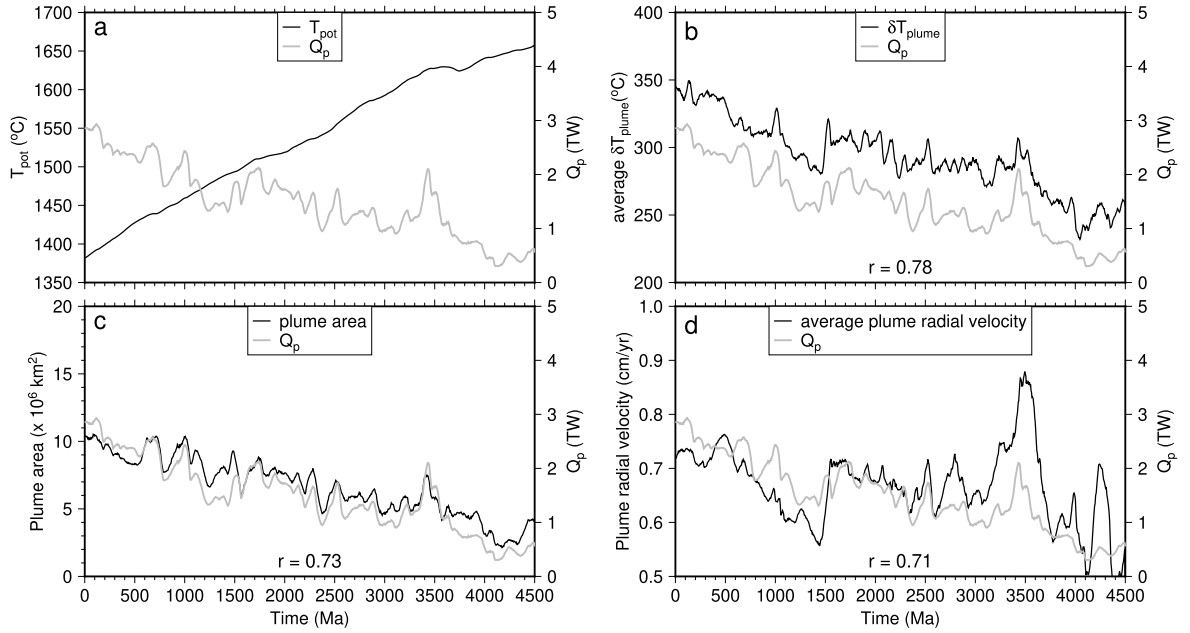

Fig. 5. Time evolution of total plume heat flux Q_p and average mantle potential temperature T_{pot} (a), average plume excess temperature (b), total area of plumes (c), and average plume radial velocity (d) for case 1. Plumes are defined at 700 km deep using f=0.06, e.g., a minimum plume excess temperature of δT_{plume}=200 °C. The r value in panels (b-d) shows the correlation coefficient between the two curves in each panel, which is calculated after the linear trends are removed.

frequently than case 1 (Fig. 8a). The secular variation of Q_p shows periodicities of 312, 180, 135, 128 and 92 Myr above the 95% confidence level (Fig. 8b) and the periodicity of 312 Myr is above the 99% confidence level. The variation of u_0^{rms} has a periodicity of 613 Myr above the 99% confidence level (Fig. 8c).

Case 5 uses a different initial mantle temperature structure with higher T_{pot} of 1710 °C at 4500 Ma, which decreases to ~1450 °C at 0 Ma (Supplementary Information Figure S1a, Supplementary Information Table S3). Compared to case 1, Q_p in case 5 is slightly lower (Fig. 9a), because of the reduced plume excess temperature as the background mantle becomes hotter. The variation of Q_p has a periodicity of 237 Myr above the 99% confidence level and another periodicity of 152 Myr above the 95% confidence level (Fig. 9b). The variation of u_0^{rms} is dominated by a periodicity of 532 Myr that is above the 99% confidence level (Fig. 9c).

4. Discussion

In this study, we analyze 3D global mantle convection models, and we examine the secular variations of the total plume heat flux Q_p and the rms of the surface velocity u_0^{rms}. Fig. 10 compares the periodicities of the variations of Q_p and the u_0^{rms} versus the average of the rms of the surface velocity ($\overline{u_0^{rms}}$) and the average of the rms of the global mantle flow velocity ($\overline{u_{wm}^{rms}}$) from 3000 Ma to 0 Ma for cases 1-5. We find that all cases show multiple periodicities in the variation of Q_p which generally decrease with $\overline{u_0^{rms}}$ and $\overline{u_{wm}^{rms}}$. A periodicity is also observed in the variation of u_0^{rms} for each case which also decreases with $\overline{u_0^{rms}}$ and $\overline{u_{wm}^{rms}}$.

The Earth has an average plate velocity of ~4-5 cm/yr at the present-day. It varies with time and may be up to several times higher in the past 1 Ga (Müller et al., 2022). Compared to Earth's plate velocity, the surface velocity in all our models is much smaller. We find that the $\overline{u_{wm}^{rms}}$ of cases 1, 4 and 5 are significantly higher than case 2 (Fig. 10b) which is not surprising because these cases have 2× higher Rayleigh number than case 2; however, all these four cases have the similar $\overline{u_0^{rms}}$. This result indicates that the surface motions in (at least some of) our models remain sluggish and are not fully mobile, which may be because our simulations of the lithospheric deformation remain too simplified compared to the complex Earth. Therefore, we argue that, in our models, the global mantle flow velocity better represents the vigor of mantle convection than the surface velocity.

Compared to Earth's plate motion at the surface, the Earth's global mantle flow velocity is less well constrained, but studies based on the depths of subducted slabs from tomography models and estimations of slab ages have suggested an average sinking rate of ~1.2 cm/yr for subducted slabs in the most recent ~250 Ma (van der Meer et al., 2011). Because mantle flow velocity is generally higher in subducted slabs than in the background mantle and because the background mantle has much more volume than subducted slabs, the rms of the Earth's global mantle flow in the past ~250 Ma may be lower than ~1.0 cm/yr. Therefore, we may use $\overline{u_{wm}^{rms}}$ = 0.8 cm/yr to represent a condition with Earth-like vigor of mantle convection in the past ~250 Ma. As shown in Fig. 10b, the $\overline{u_{wm}^{rms}}$ in our models range from 0.33 in case 2 to 0.69 cm/yr in case 3. The periodicities of the Q_p decrease rapidly with $\overline{u_{wm}^{rms}}$ when $\overline{u_{wm}^{rms}}$ is less than 0.5 cm/yr, but when u_{wm}^{rms} is larger than 0.5 cm/yr, the rate of decrease is greatly reduced and the trend curves tend to be asymptotic. Following this trend, the periodicities of the Q_p may be in a range of ~90-200 Myr for $\overline{u_{wm}^{rms}}$ at 0.8 cm/yr, which is in good agreement with previous studies of ~100-200 Myr for the periodicities of individual plumes (Le Bars and Davaille, 2004; Davaille et al., 2005; Li et al., 2018). As shown in Fig. 10b, the periodicity of u_0^{rms} decreases linearly with $\overline{u_{wm}^{rms}}$, and following this trend, it will have a periodicity of ~300 Myr when $\overline{u_{wm}^{rms}}$ is at 0.8 cm/yr. Note that our definition of Earth's vigor of deep mantle convection at $\overline{u_{wm}^{rms}}$ = 0.8 cm/yr is arbitrary, although it is based on previous estimations on the sinking rate of subducted slabs (van der Meer et al., 2011). If Earth's vigor of deep mantle convection is higher, especially in the earlier history due to higher mantle temperature and thus lower mantle viscosity, the periodicity of u_0^{rms} might decrease following the linear trend line in Fig. 10d, but the periodicities of the Q_p won't be significantly affected according to the trend lines in Fig. 10b that tend to be asymptotic at large u_{wm}^{rms}.

It is well known that the spectrum of any time series can have periods where the spectral powers are at local maxima, except for

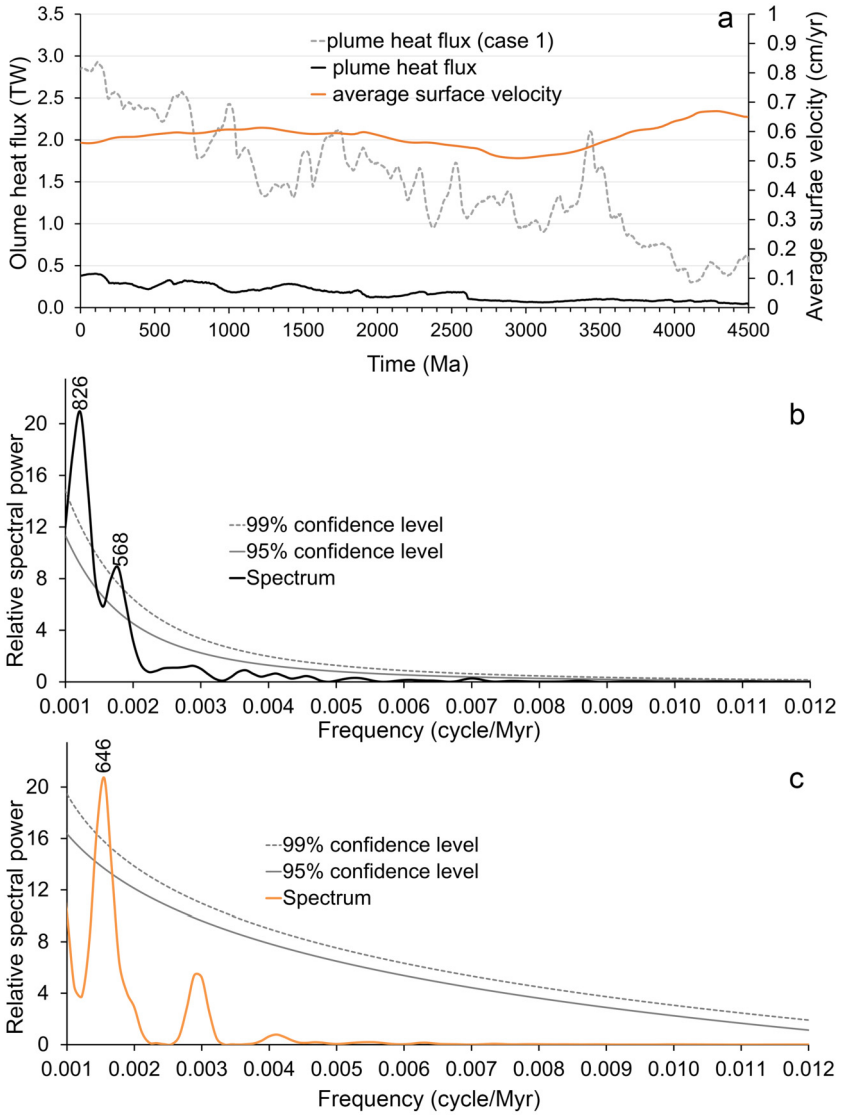

Fig. 6. a, Time evolution of the total plume heat flux Q_p (black) quantified with f=0.06 at 700 km depth, and the root-mean square of surface velocity (orange) or u_0^{rms} for case 2 with lower Rayleigh number. b, Power spectrum of Q_p. c, Power spectrum of u_0^{rms}. In panels (b) and (c), numbers above the peaks refer to periodicities whose magnitudes are above the 95% confidence level. Spectral analyses are performed at 3000-0 Ma after the linear trends are removed. The dashed gray curve in panel (a) shows the Q_p quantified with f=0.06 at 700 km depth for case 1.

white noise and red noise. Therefore, confidence levels are often calculated to determine to what extent a periodicity is credible. In statistics, a periodicity whose confidence level is higher than 95% or 99% is probably real. In this study, all the periodicities for the variation of Q_p are above the 95% confidence level with many of them above the 99% confidence level (Figs. 3, 6–9), indicating that these periodicities are probably real.

However, it is possible that even random number sequences can coincidently show periodicities above 95% confidence level. One way to determine if a periodicity is significant or caused by coincidence is to perform spectrum analysis on new independent data. Puetz and Condie (2022) tested four independent global detrital zircon databases (Voice et al., 2011; Roberts and Spencer, 2015; Puetz and Condie, 2019; Puetz et al., 2021), and found all these databases show nearly identical periodicities above the 95% confidence level. Therefore, the periodicities in the detrital zircon age distributions are consistently reproducible at high confidence levels from four independent databases and are thus different from random number sequences whose periodicities are random and different for every new dataset.

Different from the detrital zircon age distribution whose periodicities can be confirmed by using multiple datasets, mantle dynamics and thus the periodicities of the variations of the total plume heat flux Q_p are model-dependent, and we acknowledge that any mantle convection model could produce a time series of plume heat flux that shows some periodic cycles. So, the question is: what is special for the periodicities of the Q_p in this study and why do we care about them? The answer is that some key measurements in our models are consistent with Earth's observations; therefore, results of our models are relevant and have important implications for Earth's deep processes. Specifically, when using f=0.03-0.09 or a threshold plume excess temperature of 100-300 °C to define plume regions, which generally agrees with the plume excess temperature beneath plume-generated hotspots (e.g., Schilling, 1991), most of our models (except case 2) show present-day Q_p of ~2-5 TW which is similar to the Q_p estimated for the Earth (e.g., Sleep, 1990; Davies, 1993). Our models also produce Earth-like evolution of mantle potential temperature (Supplementary Information Figure S1a). Furthermore, results of our models can be extrapolated to conditions with Earth-like vigor of convec-

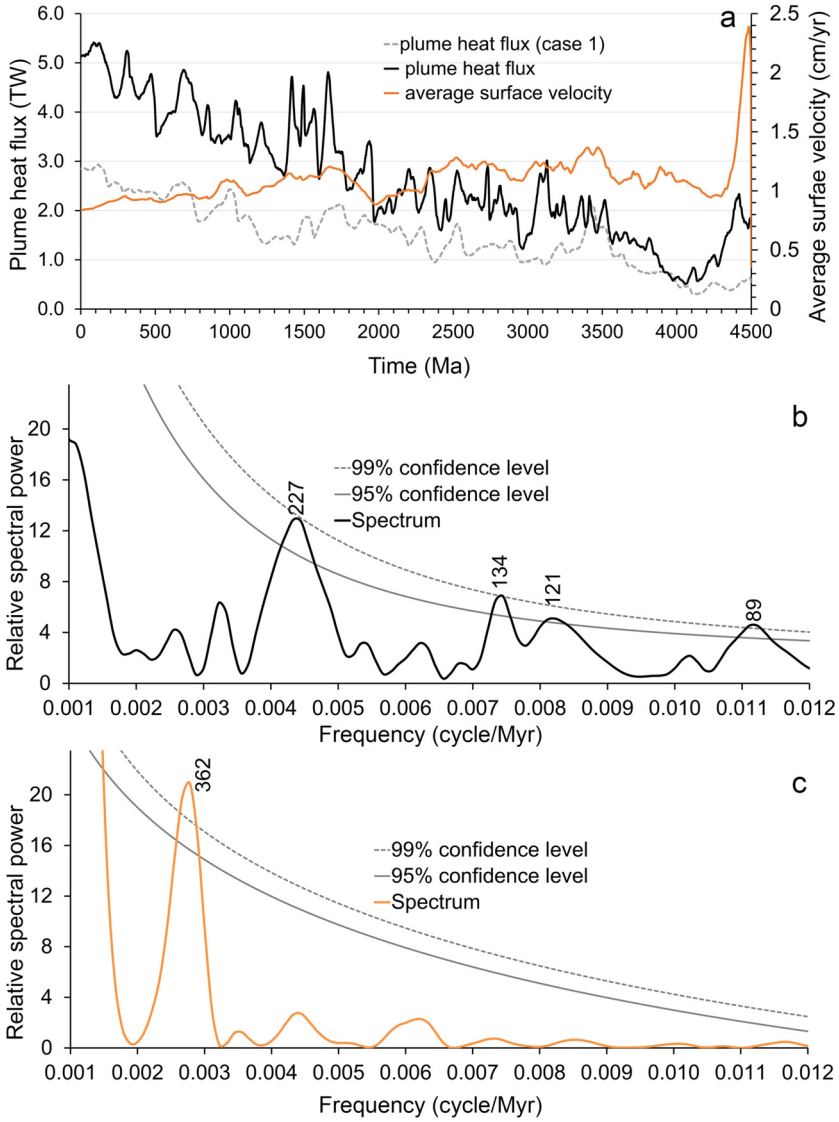

Fig. 7. Same as Fig. 6 except for case 3 with higher Rayleigh number.

tion as shown in Fig. 10. Because of these features of our models, it is reasonably safe to argue that our modeling results are applicable to the true Earth. Our results suggest that the plume heat flux in Earth's mantle may have multiple periodicities in the range of ~90-200 Myr. Interestingly, periodicities at 89, 103, 107, 136, 170 and 188 Myr have also been found in the global detrital zircon age distribution A_{zir}, all within the range of ~90-200 Myr. This result suggests these periodicities in A_{zir} can be due to plume-induced magmatism.

Besides mantle plumes, the continental crust is also produced by arc volcanism at subduction zones (Rudnick, 1995; Hawkesworth et al., 2010). It has been proposed that pulses of continental crust growth may result from periods of accelerated plate motion and subduction rate in Earth's history (O'Neill et al., 2007; Arndt and Davaille, 2013). As a test, we also quantify the root-mean-squares of the surface velocities (u_0^{rms}) in our models. We find that the periodicity of the variation of u_0^{rms} decreases linearly with $\overline{u_{wm}^{rms}}$ (Fig. 10d). Our results suggest a periodicity of around 300 Myr for the temporal variation of u_0^{rms} after extrapolating our results to a regime with Earth-like $\overline{u_{wm}^{rms}}$ of 0.8 cm/yr (Fig. 10d). Interestingly, a periodicity of 312 Myr has been found in the detrital zircon age distribution (Fig. 1b), which suggests that this periodicity may be related to the temporal variation of surface motion. Since the melt production rate of arc magmatism is directly related to the surface motion (e.g., O'Neill et al., 2007), our results suggest that the temporal variation of the surface motion may have contributed to the ~300 Myr periodic cycle for the growth of continental crust. It needs to be pointed out that although the magnitude of u_0^{rms} is low which may be due to the simplified rheology laws used in our models, the temporal variation of the u_0^{rms} closely follows the variation of the global mantle flow velocity (Fig. 3a) that better represents the vigor of mantle convection; therefore, the periodicity of the u_0^{rms} may be less affected by the model simplification than its low magnitude.

We stress that the evolution of Earth's mantle is complex and may also have been affected by other factors not included in our models. First, our models do not include the assemblage and breakup of supercontinents (e.g., Zhong et al., 2007; Rolf et al., 2014). The cycle of 802 Myr in the global detrital zircon age distribution (Fig. 1b), which is not observed nor predicted in the periodicities of the variations of Q_p and u_0^{rms} in our models, may be related to the supercontinent cycle, as suggested by Korenaga (2006). Due to the lack of continents, our models do not have the Wilson cycle which have been suggested to have a periodicity of

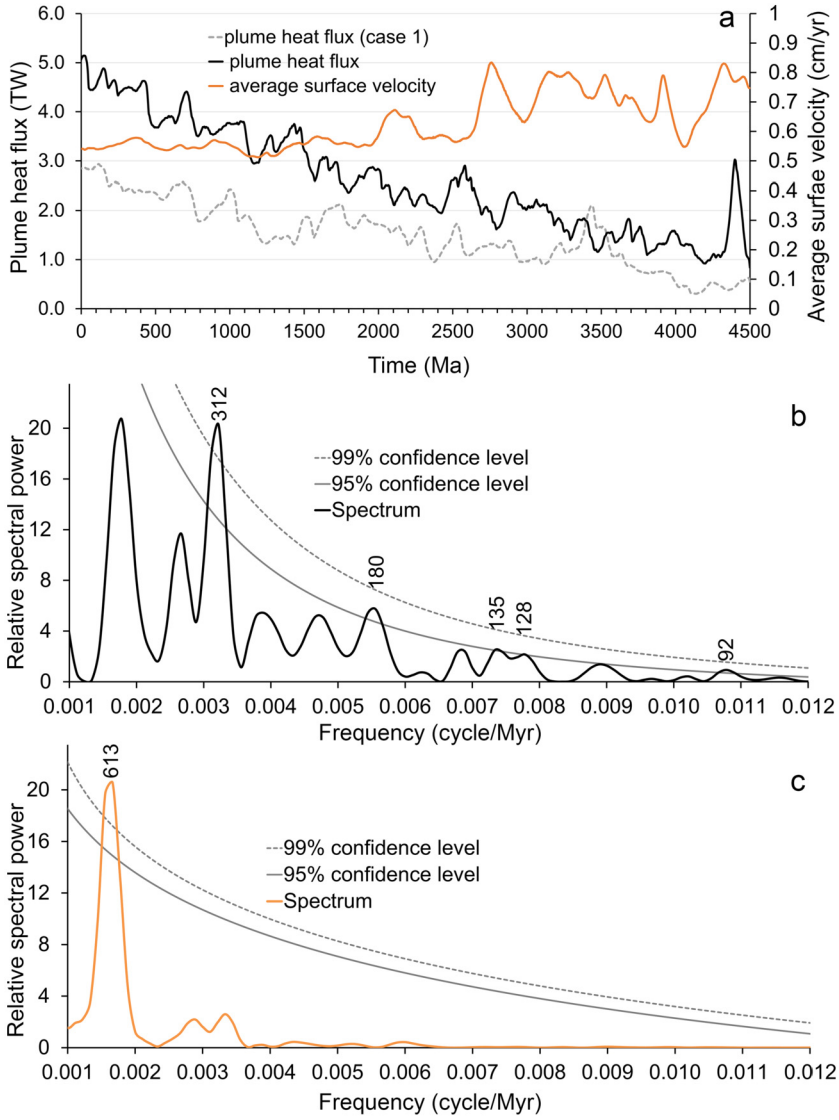

Fig. 8. Same as Fig. 6 but for case 4 with higher degree of temperature-dependent viscosity.

~200-350 Myr (Mitchell et al., 2019). The Wilson cycle may have also contributed to the periodic production of arc magmatism and the periodic growth of the continental crust.

Second, it has been proposed that subducted slabs could temporarily accumulate at ~660 km depth before episodically sinking to the lower mantle (e.g., Peltier and Solheim, 1992; Tackley et al., 1993; Davies, 1995, 2008; Wolstencroft and Davies, 2011; Wang and Li, 2020; Yuan and Li, 2022) - a process often referred to as slab avalanches. Our models include a Clapeyron slope -2.9 MPa/K for the 660 km phase transition and a 30× viscosity increase at 660 km depth from upper to lower mantle, but we do not observe slab avalanche events (Supplementary Information Movie S1). This may be because the Rayleigh number in our models and thus the vigor of convection remains lower than the Earth as indicated by the low mantle flow velocity in our models (Fig. 10), and as a result, subducted slabs in our models may be too thick to become stagnant at the 660 km depth. In addition, whereas the increase of viscosity occurs at a constant depth of 660 km in our models, the depth for the density increase due to the post-spinel phase transition moves up and down around 660 km depth. By increasing the viscosity at the same depths where the density increases, slab stagnation at 660 km depth might be promoted. This could lead to the occurrence of slab avalanche events. Nevertheless, seismic observations have clearly shown some subducted slabs being strongly deflected at the base of mantle transition zone (e.g., Fukao et al., 1992), suggesting that slab avalanche events are likely part of Earth's history of mantle convection. Previous studies have shown that mantle overturn due to slab avalanche events can be episodic, with a wide range of periodicities from 100's Myr to ~1.0 Gyr (e.g., Davies, 1995). Thus, the 500 Myr periodic cycle in the detrital zircon age distribution may be related to slab avalanche events. Even without slab avalanche events, the arrivals of new subducted slabs to the lowermost mantle or the temporal changes of subduction flux could perturb the basal TBL and trigger the formation of mantle plumes and thus affect plume heat flux (e.g., Tan et al., 2002, 2011; Steinberger and Torsvik, 2012; Li and Zhong, 2017). In our models, the variation of the plume heat flux results from the interactions between subducted slabs and the basal TBL and the interactions between plumes and the surrounding mantle. That is, the influence of subducted slabs on the formation of mantle plumes is implicitly included in our models.

Third, the rheology of Earth's mantle is more complex than in our models, including larger activation energy for temperature-dependent viscosity (Kohlstedt and Hansen, 2015), and stress and grain-size dependence of viscosity (Karato and Wu, 1993; Solomatov and Reese, 2008; Dannberg et al., 2017). We find that an

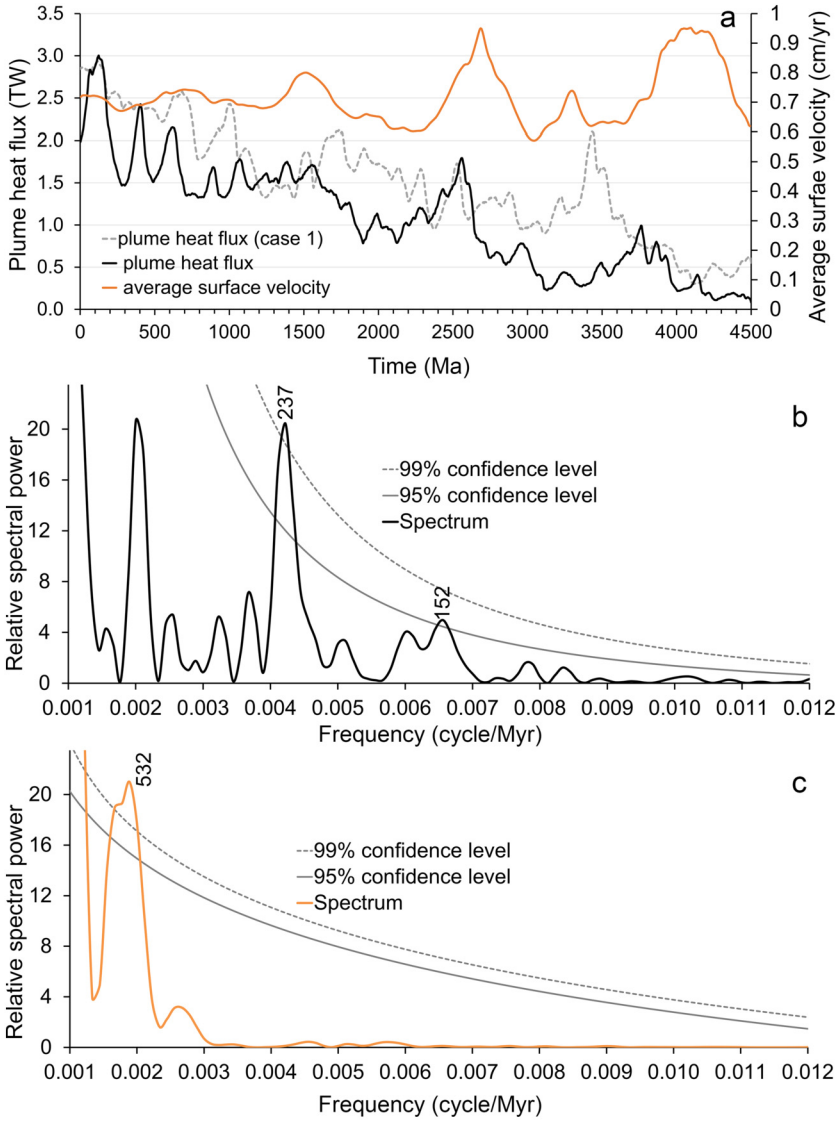

Fig. 9. Same as Fig. 6 except for case 5 with higher initial mantle temperature.

increase of activation energy leads to more frequent formation of plumes and shorter periods for the variation of the total plume heat flux (e.g., Fig. 8). However, previous studies found that for an activation energy of 500 kJ/mol or higher, small-scale convection may first develop in the basal TBL before the development of large plumes (Thompson and Tackley, 1998; Solomatov and Moresi, 2002); and if so, we expect that large plumes may form less frequently. The stress- and grain-size- dependence of viscosity could significantly affect mantle dynamics (Foley and Bercovici, 2014; Dannberg et al., 2017) and morphology of plumes (Davaille et al., 2018), but its effects on the periodicities of plume heat flux and surface velocity are less clear. Without considering continents and by using simplified rheological laws, our models do not generate realistic plate behaviors. Producing realistic plate behaviors remains a grand challenge in geodynamic modeling studies, even though significant progresses have been made in the past (e.g., see review by Bercovici et al., 2015). In our models, the temporal variation of u_0^{rms} follows the temporal variation of u_{wm}^{rms} and is much smoother than the variation of the rms of plate velocity for the Earth that contains abrupt changes (Müller et al., 2022). Therefore, periodicities less than ~300 Myr for the temporal variation of the rms of the plate velocity for the Earth are not excluded by our models.

Fourth, the Earth's lowermost mantle may contain intrinsically dense chemical heterogeneities, which may be pushed by convection into thermochemical piles (McNamara and Zhong, 2004; Li and McNamara, 2018; Li et al., 2018). The presence of thermochemical piles on the CMB may affect the excess temperature of plumes (e.g., Farnetani, 1997; Tan et al., 2011; Li and Zhong, 2017). Previous 2D geodynamic models have also shown that the morphology of thermochemical piles may change periodically in response to changes in subduction rates, which could trigger or be accompanied by periodic increases in heat flux in existing plumes or the formation of new mantle plumes (Li et al., 2018; Heyn et al., 2020).

Finally, we hypothesize that the production rate of magma is, to the first order, controlled by heat flux of plumes and subduction rate (which is related to surface velocity), as suggested by previous studies (e.g., O'Neill et al., 2007; Arndt and Davaille, 2013; Wang and Li, 2021). However, the rate of melt production is affected by mantle chemical heterogeneities as well (e.g., Langmuir et al., 1992; Li et al., 2016), and the production of continental crust involves complex process of melt migration. These factors are not explicitly simulated in this study. It is beyond the scope of this study to explore all the complexities listed above, and therefore, our results do not exclude other mechanisms that may have con-

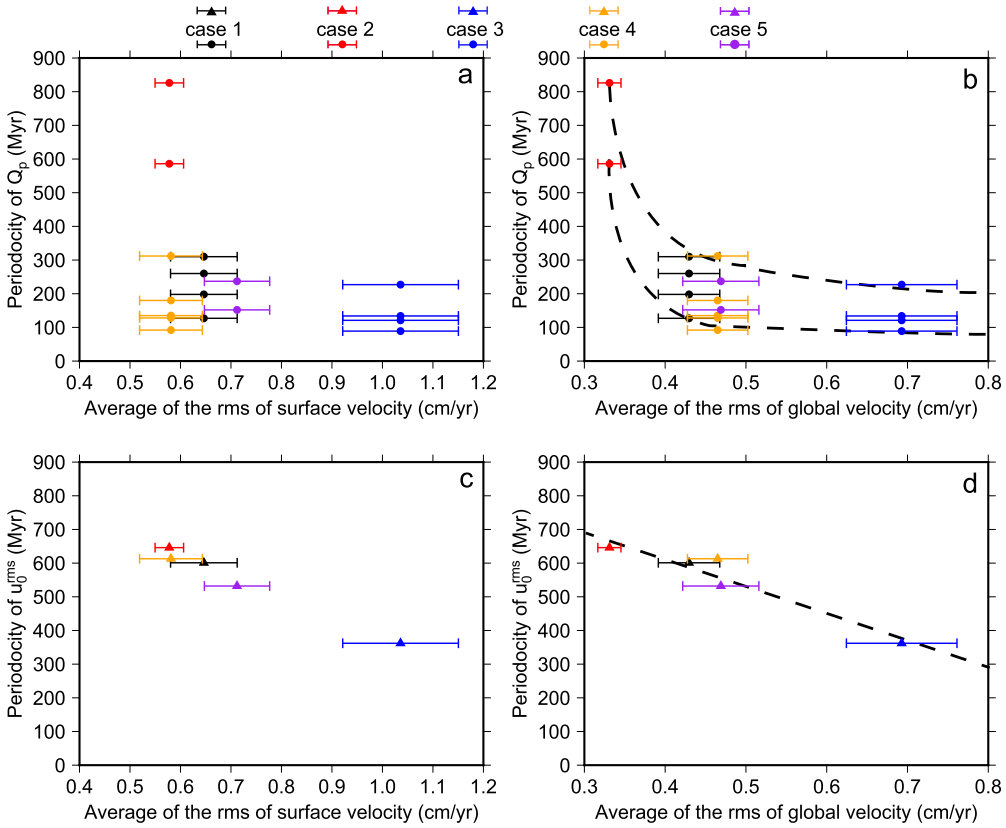

Fig. 10. a-b, The periodicities of the Q_p versus (a) the average rms of the surface velocity or $\overline{u_0^{rms}}$ and (b) the average rms of the global mantle flow velocity or $\overline{u_{wm}^{rms}}$, in the past 3000 Ma for case 1 (black), case 2 (red), case 3 (blue), case 4 (orange) and case 5 (purple). c-d, same as panels a-b but the periodicities of the u_0^{rms} are compared to (c) $\overline{u_0^{rms}}$ and (d) $\overline{u_{wm}^{rms}}$. The Q_p is calculated at 700 km depth using f=0.06. The error bars show the standard deviations of $\overline{u_0^{rms}}$ and $\overline{u_{wm}^{rms}}$. Black dashed curves in panels (b) and (d) are added to show the general trends.

tributed to the periodic cycles of the plume heat flux, the rms of the surface velocity, and the periodic growth of the continental crust.

5. Conclusion

In this study, we perform 3D global geodynamic modeling experiments to study the long-term variations of plume heat flux and the surface flow velocity, which respectively relate to plume-induced magmatism and arc magmatism – the two major mechanisms for the production of continental crust. Our models are run throughout Earth's history with the mantle potential temperature decreasing monotonically with time, and they also have Earth-like plume excess temperatures, total plume heat flux, and mantle thermal evolution. We find that both the temporal variations of the total plume heat flux and the root-mean-square (rms) of the surface velocity in our models have periodicities that decrease with the vigor of mantle convection. When extrapolated to conditions with Earth-like vigor of convection, the total plume heat flux and the rms of the surface velocity vary with periodic cycles of ~90-200 Myr and ~300 Myr, respectively. Therefore, the periodicities at ~90-200 Myr and ~300 Myr in the growth of continental crust as suggested by the analysis of the global detrital zircon U-Pb age distribution may be caused by plume-induced magmatism and arc magmatism, respectively.

CRediT authorship contribution statement

Mingming Li: Conceptualization, Methodology, Investigation, Writing, Visualization. **Steven Puetz:** Conceptualization, Investigation, Writing. **Kent Condie:**Kent Condie: Conceptualization, Writing. **Peter Olson:** Conceptualization, Writing.

Declaration of competing interest

The authors declare that they have no known competing financial interests or personal relationships that could have appeared to influence the work reported in this paper.

Data availability

A link for the open source CitcomS code used in this study is provided in the Acknowledgments section.

Acknowledgements

This work benefits from supports of National Science Foundation (NSF) grants EAR-2216564, EAR-2054926, and EAR-1849949. The CitcomS code used in this work is open source and is available at http://geoweb.cse.ucdavis.edu/cig/software/citcoms/. We thank Paul Tackley and an anonymous reviewer for their constructive comments.

Appendix A. Supplementary material

Supplementary material related to this article can be found online at https://doi.org/10.1016/j.epsl.2023.118148.

References

Abbott, D., Burgess, L., Longhi, J., Smith, W.H.F., 1994. An empirical thermal history of the Earth's upper mantle. J. Geophys. Res. 99, 13835–13850. https://doi.org/10.1029/94JB00112.

Albarède, F., 1998. The growth of continental crust. Tectonophysics 296, 1–14. https://doi.org/10.1016/S0040-1951(98)00133-4.

Armstrong, R.L., Harmon, R.S., 1981. Radiogenic isotopes: the case for crustal recycling on a near-steady-state no-continental-growth Earth [and discussion]. Philos. Trans. R. Soc. Lond. Ser. A, Math. Phys. Sci. 301, 443–472. https://doi.org/10.1098/rsta.1981.0122.

Arndt, N., Davaille, A., 2013. Episodic Earth evolution. Tectonophysics 609, 661–674. https://doi.org/10.1016/j.tecto.2013.07.002.

Arnould, M., Coltice, N., Flament, N., Mallard, C., 2020. Plate tectonics and mantle controls on plume dynamics. Earth Planet. Sci. Lett. 547, 116439. https://doi.org/10.1016/j.epsl.2020.116439.

Bercovici, D., Tackley, P.J., Ricard, Y., 2015. The generation of plate tectonics from mantle dynamics. In: Schubert, G. (Ed.), Treatise on Geophysics. Elsevier, Oxford, pp. 271–318.

Condie, K.C., Arndt, N., Davaille, A., Puetz, S.J., 2017. Zircon age peaks: production or preservation of continental crust? Geosphere 13, 227–234. https://doi.org/10.1130/ges01361.1.

Condie, K.C., Aster, R.C., 2010. Episodic zircon age spectra of orogenic granitoids: the supercontinent connection and continental growth. Precambrian Res. 180, 227–236. https://doi.org/10.1016/j.precamres.2010.03.008.

Condie, K.C., Davaille, A., Aster, R.C., Arndt, N., 2014. Upstairs-downstairs: supercontinents and large igneous provinces, are they related? Int. Geol. Rev. 57, 1341–1348. https://doi.org/10.1080/00206814.2014.963170.

Courtillot, V., Davaille, A., Besse, J., Stock, J., 2003. Three distinct types of hotspots in the Earth's mantle. Earth Planet. Sci. Lett. 205, 295–308. https://doi.org/10.1016/S0012-821x(02)01048-8.

Dalton, C.A., Langmuir, C.H., Gale, A., 2014. Geophysical and geochemical evidence for deep temperature variations beneath mid-ocean ridges. Science 344, 80–83. https://doi.org/10.1126/science.1249466.

Dannberg, J., Eilon, Z., Faul, U., Gassmöller, R., Moulik, P., Myhill, R., 2017. The importance of grain size to mantle dynamics and seismological observations. Geochem. Geophys. Geosyst. 18, 3034–3061. https://doi.org/10.1002/2017GC006944.

Davaille, A., Carrez, P., Cordier, P., 2018. Fat plumes may reflect the complex rheology of the lower mantle. Geophys. Res. Lett. 45, 1349–1354. https://doi.org/10.1002/2017gl076575.

Davaille, A., Stutzmann, E., Silveira, G., Besse, J., Courtillot, V., 2005. Convective patterns under the Indo-Atlantic <box>? Earth Planet. Sci. Lett. 239, 233–252. https://doi.org/10.1016/j.epsl.2005.07.024.

Davies, G.F., 1993. Cooling the core and mantle by plume and plate flows. Geophys. J. Int. 115, 132–146. https://doi.org/10.1111/j.1365-246X.1993.tb05593.x.

Davies, G.F., 1995. Punctuated tectonic evolution of the Earth. Earth Planet. Sci. Lett. 136, 363–379. https://doi.org/10.1016/0012-821X(95)00167-B.

Davies, G.F., 2008. Episodic layering of the early mantle by the 'basalt barrier' mechanism. Earth Planet. Sci. Lett. 275, 382–392. https://doi.org/10.1016/j.epsl.2008.08.036.

Duffy, T.S., Ahrens, T.J., 1993. Thermal-expansion of mantle and core materials at very high-pressures. Geophys. Res. Lett. 20, 1103–1106. https://doi.org/10.1029/93gl00479.

Farnetani, C.G., 1997. Excess temperature of mantle plumes: the role of chemical stratification across D″. Geophys. Res. Lett. 24, 1583–1586. https://doi.org/10.1029/97gl01548.

Foley, B.J., Bercovici, D., 2014. Scaling laws for convection with temperature-dependent viscosity and grain-damage. Geophys. J. Int. 199, 580–603. https://doi.org/10.1093/gji/ggu275.

Fukao, Y., Obayashi, M., Inoue, H., Nenbai, M., 1992. Subducting slabs stagnant in the mantle transition zone. J. Geophys. Res., Solid Earth 97, 4809–4822. https://doi.org/10.1029/91jb02749.

Hawkesworth, C.J., Dhuime, B., Pietranik, A.B., Cawood, P.A., Kemp, A.I.S., Storey, C.D., 2010. The generation and evolution of the continental crust. J. Geol. Soc. 167, 229–248. https://doi.org/10.1144/0016-76492009-072.

Herzberg, C., Condie, K., Korenaga, J., 2010. Thermal history of the Earth and its petrological expression. Earth Planet. Sci. Lett. 292, 79–88. https://doi.org/10.1016/j.epsl.2010.01.022.

Heyn, B.H., Conrad, C.P., Trønnes, R.G., 2020. How thermochemical piles can (periodically) generate plumes at their edges. J. Geophys. Res. 125, e2019JB018726. https://doi.org/10.1029/2019JB018726.

Hofmeister, A.M., 1999. Mantle values of thermal conductivity and the geotherm from phonon lifetimes. Science 283, 1699–1706. https://doi.org/10.1126/science.283.5408.1699.

Howard, L.N., 1966. Convection at high Rayleigh number. In: Görtler, H. (Ed.), Applied Mechanics: Proceedings of the Eleventh International Congress of Applied Mechanics Munich (Germany) 1964. Springer Berlin Heidelberg, Berlin, Heidelberg, pp. 1109–1115.

Karato, S., Wu, P., 1993. Rheology of the upper mantle - a synthesis. Science 260, 771–778. https://doi.org/10.1126/science.260.5109.771.

Kohlstedt, D.L., Hansen, L.N., 2015. 2.18 - Constitutive equations, rheological behavior, and viscosity of rocks. In: Schubert, G. (Ed.), Treatise on Geophysics, second edition. Elsevier, Oxford, pp. 441–472.

Korenaga, J., 2006. Archean geodynamics and the thermal evolution of Earth. In: Benn, K., Mareschal, J.-C., Condie, K. (Eds.), AGU Geophysical Monograph Series. AGU, Washington DC, pp. 7–32.

Langmuir, C.H., Klein, E.M., Plank, T., 1992. Petrological systematics of mid-ocean ridge basalts: constraints on melt generation beneath ocean ridges. In: Mantle Flow and Melt Generation at Mid-Ocean Ridges. American Geophysical Union, pp. 183–280.

Le Bars, M., Davaille, A., 2004. Large interface deformation in two-layer thermal convection of miscible viscous fluids. J. Fluid Mech. 499, 75–110. https://doi.org/10.1017/S0022112003006931.

Leng, W., Zhong, S.J., 2008. Controls on plume heat flux and plume excess temperature. J. Geophys. Res. 113, B04408. https://doi.org/10.1029/2007jb005155.

Li, M., Black, B., Zhong, S., Manga, M., Rudolph, M.L., Olson, P., 2016. Quantifying melt production and degassing rate at mid-ocean ridges from global mantle convection models with plate motion history. Geochem. Geophys. Geosyst. 17, 2884–2904. https://doi.org/10.1002/2016gc006439.

Li, M., McNamara, A.K., 2018. The influence of deep mantle compositional heterogeneity on Earth's thermal evolution. Earth Planet. Sci. Lett. 500, 86–96. https://doi.org/10.1016/j.epsl.2018.08.009.

Li, M., Zhong, S.J., 2017. The source location of mantle plumes from 3D spherical models of mantle convection. Earth Planet. Sci. Lett. 478, 47–57. https://doi.org/10.1016/j.epsl.2017.08.033.

Li, M., Zhong, S., 2019. Lateral motion of mantle plumes in 3-D geodynamic models. Geophys. Res. Lett. 46, 4685–4693. https://doi.org/10.1029/2018gl081404.

Li, M., Zhong, S.J., Olson, P., 2018. Linking lowermost mantle structure, core-mantle boundary heat flux and mantle plume formation. Phys. Earth Planet. Inter. 277, 10–29. https://doi.org/10.1016/j.pepi.2018.01.010.

Lin, S.C., van Keken, P.E., 2005. Multiple volcanic episodes of flood basalts caused by thermochemical mantle plumes. Nature 436, 250–252. https://doi.org/10.1038/Nature03697.

McNamara, A.K., Zhong, S.J., 2004. Thermochemical structures within a spherical mantle: superplumes or piles? J. Geophys. Res., Solid Earth 109, B07402. https://doi.org/10.1029/2003jb002847.

Mitchell, R.N., Spencer, C.J., Kirscher, U., He, X.-F., Murphy, J.B., Li, Z.-X., Collins, W.J., 2019. Harmonic hierarchy of mantle and lithospheric convective cycles: time series analysis of hafnium isotopes of zircon. Gondwana Res. 75, 239–248. https://doi.org/10.1016/j.gr.2019.06.003.

Müller, R.D., Flament, N., Cannon, J., Tetley, M.G., Williams, S.E., Cao, X., Bodur, Ö.F., Zahirovic, S., Merdith, A., 2022. A tectonic-rules-based mantle reference frame since 1 billion years ago – implications for supercontinent cycles and plate–mantle system evolution. Solid Earth 13, 1127–1159. https://doi.org/10.5194/se-13-1127-2022.

O'Neill, C., Lenardic, A., Moresi, L., Torsvik, T.H., Lee, C.T.A., 2007. Episodic Precambrian subduction. Earth Planet. Sci. Lett. 262, 552–562. https://doi.org/10.1016/j.epsl.2007.04.056.

Olson, P., 1993. Hot spots, swells and mantle plumes. In: Ryan, M.P. (Ed.), Magma Transport and Storage. John Wiley, New York, pp. 33–51.

Peltier, W.R., Solheim, L.P., 1992. Mantle phase transitions and layered chaotic convection. Geophys. Res. Lett. 19, 321–324. https://doi.org/10.1029/91GL02951.

Puetz, S.J., Condie, K.C., 2019. Time series analysis of mantle cycles part I: periodicities and correlations among seven global isotopic databases. Geosci. Front. 10, 1305–1326. https://doi.org/10.1016/j.gsf.2019.04.002.

Puetz, S.J., Condie, K.C., 2022. A review of methods used to test periodicity of natural processes with a special focus on harmonic periodicities found in global U Pb detrital zircon age distributions. Earth-Sci. Rev. 224, 103885. https://doi.org/10.1016/j.earscirev.2021.103885.

Puetz, S.J., Spencer, C.J., Ganade, C.E., 2021. Analyses from a validated global U-Pb detrital zircon database: enhanced methods for filtering discordant U-Pb zircon analyses and optimizing crystallization age estimates. Earth-Sci. Rev. 220, 103745. https://doi.org/10.1016/j.earscirev.2021.103745.

Roberts, N.M.W., Spencer, C.J., 2015. The zircon archive of continent formation through time. Geol. Soc. (Lond.) Spec. Publ. 389, 197–225. https://doi.org/10.1144/sp389.14.

Rolf, T., Coltice, N., Tackley, P.J., 2014. Statistical cyclicity of the supercontinent cycle. Geophys. Res. Lett. 41, 2351–2358. https://doi.org/10.1002/2014gl059595.

Rudnick, R.L., 1995. Making continental-crust. Nature 378, 571–578. https://doi.org/10.1038/378571a0.

Schilling, J.-G., 1991. Fluxes and excess temperatures of mantle plumes inferred from their interaction with migrating mid-ocean ridges. Nature 352, 397–403. https://doi.org/10.1038/352397a0.

Schulz, M., Mudelsee, M., 2002. REDFIT: estimating red-noise spectra directly from unevenly spaced paleoclimatic time series. Comput. Geosci. 28, 421–426. https://doi.org/10.1016/s0098-3004(01)00044-9.

Sleep, N.H., 1990. Hotspots and mantle plumes: some phenomenology. J. Geophys. Res. 95, 6715–6736. https://doi.org/10.1029/JB095iB05p06715.

Solomatov, V.S., Moresi, L.N., 2002. Small-scale convection in the D″ layer. J. Geophys. Res., Solid Earth 107, ETG 3-1–ETG 3-10. https://doi.org/10.1029/2000jb000063.

Solomatov, V., Reese, C., 2008. Grain size variations in the Earth's mantle and the evolution of primordial chemical heterogeneities. J. Geophys. Res., Solid Earth, B07408. https://doi.org/10.1029/2007JB005319.

Steinberger, B., Torsvik, T.H., 2012. A geodynamic model of plumes from the margins of Large Low Shear Velocity Provinces. Geochem. Geophys. Geosyst. 13, Q01W09. https://doi.org/10.1029/2011gc003808.

Stern, R.J., Scholl, D.W., 2010. Yin and Yang of continental crust creation and destruction by plate tectonic processes. Int. Geol. Rev. 52, 1–31. https://doi.org/10.1080/00206810903332322.

Tackley, P.J., Stevenson, D.J., Glatzmaier, G.A., Schubert, G., 1993. Effects of an endothermic phase-transition at 670 km depth in a spherical model of convection in the earths mantle. Nature 361, 699–704. https://doi.org/10.1038/361699a0.

Tan, E., Gurnis, M., Han, L., 2002. Slabs in the lower mantle and their modulation of plume formation. Geochem. Geophys. Geosyst. 3, 1–24. https://doi.org/10.1029/2001gc000238.

Tan, E., Leng, W., Zhong, S.J., Gurnis, M., 2011. On the location of plumes and lateral movement of thermochemical structures with high bulk modulus in the 3-D compressible mantle. Geochem. Geophys. Geosyst. 12, Q07005. https://doi.org/10.1029/2011gc003665.

Thompson, P.F., Tackley, P.J., 1998. Generation of mega-plumes from the core-mantle boundary in a compressible mantle with temperature-dependent viscosity. Geophys. Res. Lett. 25, 1999–2002. https://doi.org/10.1029/98GL01228.

van der Meer, D.G., Spakman, W., van Hinsbergen, D.J.J., Amaru, M.L., Torsvik, T.H., 2011. Towards absolute plate motions constrained by lower-mantle slab remnants. Nat. Geosci. 3, 36–40. https://doi.org/10.1038/ngeo708.

Voice, P.J., Kowalewski, M., Eriksson, K.A., 2011. Quantifying the timing and rate of crustal evolution: global compilation of radiometrically dated detrital zircon grains. J. Geol. 119, 109–126. https://doi.org/10.1086/658295.

Wang, Y., Li, M., 2020. Constraining mantle viscosity structure from a statistical analysis of slab stagnation events. Geochem. Geophys. Geosyst. 21, e2020GC009286. https://doi.org/10.1029/2020gc009286.

Wang, Y., Li, M., 2021. The interaction between mantle plumes and lithosphere and its surface expressions: 3-D numerical modelling. Geophys. J. Int. 225, 906–925. https://doi.org/10.1093/gji/ggab014.

Wolstencroft, M., Davies, J.H., 2011. Influence of the Ringwoodite-Perovskite transition on mantle convection in spherical geometry as a function of Clapeyron slope and Rayleigh number. Solid Earth 2, 315–326. https://doi.org/10.5194/se-2-315-2011.

Yuan, Q., Li, M., 2022. Vastly different heights of LLVPs caused by different strengths of historical slab push. Geophys. Res. Lett. 49, e2022GL099564. https://doi.org/10.1029/2022gl099564.

Zhong, S., 2006. Constraints on thermochemical convection of the mantle from plume heat flux, plume excess temperature, and upper mantle temperature. J. Geophys. Res. 111, B04409. https://doi.org/10.1029/2005jb003972.

Zhong, S., McNamara, A., Tan, E., Moresi, L., Gurnis, M., 2008. A benchmark study on mantle convection in a 3-D spherical shell using CitcomS. Geochem. Geophys. Geosyst. 9, Q10017. https://doi.org/10.1029/2008gc002048.

Zhong, S., Zhang, N., Li, Z.-X., Roberts, J.H., 2007. Supercontinent cycles, true polar wander, and very long-wavelength mantle convection. Earth Planet. Sci. Lett. 261, 551–564. https://doi.org/10.1016/j.epsl.2007.07.049.